An Accurate Determination of Motion Field and Illumination Conditions

Atsushi OSA[†a)], *Nonmember and* Hidetoshi MIIKE[†], *Member*

SUMMARY We propose a method to determine accurate motion fields and illumination conditions such as non-uniform or non-stationary illuminations. The method extends a stabilization method using reliability indices of optical flow to combine with a gradient-based approach that determines a motion field and illumination conditions simultaneously. We applied the proposed method to two synthetic image sequences and a standard image sequence. The method is effective for image sequences including poorly textured areas, edges of brightness variation, and almost dark objects.
key words: motion field, optical flow, non-uniform illumination, non-stationary illumination, stabilization

1. Introduction

Sequential image processing is useful in the fields of both computer vision and physical measurement. Determining optical flow with high accuracy is a key to technical innovation in both fields. Early studies focused on only the calculation cost to achieve real-time processing of instantaneous optical flow for robotic vision. Along with the development of computer technology, many authors have discussed the accuracy and performance of determined optical flow [1]–[6].

For accurate determination of optical flow, non-ideal conditions of image sequence are serious problems. Many approaches have been tested to determine optical flow under non-ideal conditions such as non-uniform illumination [5], [7]–[10], occlusions [11], multiple optical flows [12], non-rigid motion of objects [13], and the existence of diffusion [10], [14]. The non-ideal conditions are obstacles for determination of optical flow. However, some non-ideal conditions are important physical parameters to be fixed. Zhang et al. [5] proposed a superior approach called 'extended constraint equation with spatio-temporal local optimization (ESTO)'. ESTO determines not only accurate motion field but also illumination conditions of an image sequence. If the illumination conditions are limited to temporal non-uniform illumination, that is non-stationary illumination, 'spatio-temporal optimization method assuming discrete constance (STO-DC)' proposed by Nomura [9] can determine more accurate motion field and illumination conditions. Here, we distinguish tentatively between optical flow and the motion field. Since ESTO and STO-DC determine actual motion vectors of objects in an image sequence

of 2-dimensional plane by evaluating non-uniform or non-stationary illumination, the determined motion vectors are not optical flow itself. Optical flow is an apparent motion vector field observed in the image sequence. Here, we refer to the actual motion vectors as "Motion field." And, we call the determined illumination conditions as "Illumination parameter distribution."

On the other hand, for accurate determination of optical flow, Ohta [15] proposed a post-processing that stabilizes the determined optical flow using some reliability indices. He suggested that the stabilization method was useful when optical flow was detected without high-level knowledge about the image object. The accuracy of the determined optical flow was improved at poorly textured areas, and at areas having the aperture problem in the image.

In this paper, we propose a post-processing method that is an extension of the Ohta's stabilization method to determine motion field and illumination parameter distribution with ESTO. First, a motion field and an illumination parameter distribution are estimated from an image sequence using ESTO. Second, our proposed method evaluates their reliability indices according to the brightness distribution of the image sequence, and modifies the motion field and the illumination parameter distribution using the reliability indices with a relaxation method. We applied the proposed method to two synthetic image sequences to evaluate the improvement in accuracy. Then a standard image sequence was used to compare performances of several methods to determine motion fields. We confirmed accuracy of the proposed method and effectiveness of the stabilization.

2. Background

2.1 Determination of Motion Field and Illumination Parameter Distribution

The gradient-based approach [16] is one of the representative approaches to determine optical flow. It is based on a simple continuity equation of the image function $f(x, y, t)$ representing local gray values.

$$f_t = -f_x u_0 - f_y v_0, \qquad (1)$$

where u_0 and v_0 are the x and y components of an optical flow, and f_t, f_x, f_y are partial derivatives of the image function by t, x, and y, respectively. Although the relationship is obtained at each point on an image, one relationship is insufficient to determine two optical flow components u_0

and v_0. Therefore, in the local optimization method, a spatial [17], temporal [18] or spatio-temporal domain [19], [20] is selected on an image sequence, and it is assumed that every point in the domain has the same optical flow.

Zhang et al. [5] added a term representing non-uniform and non-stationary illuminations to the basic constraint equation, Eq. (1). Thus the extended basic constraint equation was given by

$$f_t = -f_x u - f_y v + f w, \tag{2}$$

where u and v are x and y components of a motion field taking the influences of illumination conditions into account, and w means an unknown illumination parameter [5].

They applied the spatio-temporal local optimization method and assumed u, v, and w were constant within a spatio-temporal domain consisting of $L \times M$ (pixels) and N (frames). That is, they proposed a method of determining u, v, and w by minimizing the following error function in the spatio-temporal domain:

$$E_{ESTO} = \sum_{l=0}^{L-1} \sum_{m=0}^{M-1} \sum_{n=0}^{N-1} \left(f_x u + f_y v + f_t - f w \right)^2, \tag{3}$$

where the partial derivatives are calculated at $(x+l, y+m, t+n)$, and f refers to $f(x + l, y + m, t + n)$. They called this method 'extended constraint equation with spatio-temporal local optimization (ESTO)'.

3. Stabilization Process Using Reliability Indices

3.1 Reliability Indices of Determined Motion Field and Illumination Parameter Distribution

In this section, we define reliability indices for roughly estimated motion field (u, v) and illumination parameter distribution (w). Ohta [15] proposed reliability indices for optical flow related to image texture. An optical flow (u_0, v_0) having direction θ and amplitude A can be represented as follows.

$$u_0 = A \cos \theta, \tag{4}$$

$$v_0 = A \sin \theta. \tag{5}$$

Equation (1) is given with these representations.

$$f_t = -f_x A \cos \theta - f_y A \sin \theta. \tag{6}$$

Ohta [15] assumed that every point in a spatial domain consisting of $L \times M$ (pixels) had the same motion vector, so an integration of f_t in the spatial domain was represented by F_t,

$$F_t = -A \sum_{l=0}^{L-1} \sum_{m=0}^{M-1} \left(f_x \cos \theta + f_y \sin \theta \right). \tag{7}$$

Since an optical flow of an image was determined as the norm of F_t, $\|F_t\|$, Ohta [15] clarified that the greater $\|F_t\|$ was, the more easily detectable the optical flow was, under the assumption that A was fixed. Thus, the reliability of the determined optical flow could be evaluated by the ratio of
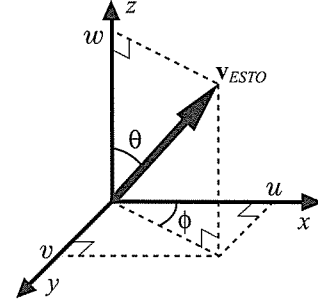
Fig. 1 Relationship between a vector $\mathbf{v}_{ESTO}$ and u, v, w.

$\|F_t\|$ to amplitude A. The ratio R was defined by

$$R = \frac{\|F_t\|}{A}. \tag{8}$$

We extend the above argument to the extended gradient-based approach of ESTO and propose reliability indices of motion field and illumination parameter distribution. Three unknown parameters (u, v, w) on ESTO can be represented by components of a 3-dimensional vector, $\mathbf{v}_{ESTO}$, in a rectangular coordinate system (see Fig. 1). When B is the amplitude of $\mathbf{v}_{ESTO}$, u, v, and w are represented by

$$u = B \sin \theta \cos \phi, \tag{9}$$

$$v = B \sin \theta \sin \phi, \tag{10}$$

$$w = B \cos \theta. \tag{11}$$

We assume that every point in the spatio-temporal domain consisting of $L \times M$ (pixels) and N (frames) has the same motion vector $\mathbf{v}(u, v)$ and the same parameter w. This assumption is equivalent to that of ESTO. Thus we get

$$\|F_t\| = \left\| B \sum_{l=0}^{L-1} \sum_{m=0}^{M-1} \sum_{n=0}^{N-1} \left(f_x C_1 + f_y C_2 - f C_3 \right) \right\|, \tag{12}$$

where $C_1 = \sin \theta \cos \phi$, $C_2 = \sin \theta \sin \phi$, and $C_3 = \cos \theta$. Then the ratios R and R^2 are represented by

$$R = \|F_t\|/B, \tag{13}$$

$$R^2 = \left\{ \sum_{l=0}^{L-1} \sum_{m=0}^{M-1} \sum_{n=0}^{N-1} \left(f_x C_1 + f_y C_2 - f C_3 \right) \right\}^2 \tag{14}$$

$$= \begin{bmatrix} C_1 & C_2 & C_3 \end{bmatrix} \begin{bmatrix} a & d & e \\ d & b & h \\ e & h & c \end{bmatrix} \begin{bmatrix} C_1 \\ C_2 \\ C_3 \end{bmatrix}. \tag{15}$$

The symbols appearing in Eq. (15) are as follows.

$$a = \sum_{l=0}^{L-1} \sum_{m=0}^{M-1} \sum_{n=0}^{N-1} f_x^2, \quad b = \sum_{l=0}^{L-1} \sum_{m=0}^{M-1} \sum_{n=0}^{N-1} f_y^2,$$

$$c = \sum_{l=0}^{L-1} \sum_{m=0}^{M-1} \sum_{n=0}^{N-1} f^2, \quad d = \sum_{l=0}^{L-1} \sum_{m=0}^{M-1} \sum_{n=0}^{N-1} f_x f_y, \tag{16}$$

$$e = -\sum_{l=0}^{L-1} \sum_{m=0}^{M-1} \sum_{n=0}^{N-1} f_x f, \quad h = -\sum_{l=0}^{L-1} \sum_{m=0}^{M-1} \sum_{n=0}^{N-1} f_y f.$$

Equation (15) is transformed into the following equation by the principal axis transformation.

$$R^2 = \begin{bmatrix} C_1 \\ C_2 \\ C_3 \end{bmatrix}^T \begin{bmatrix} \mathbf{e}_1^T \\ \mathbf{e}_2^T \\ \mathbf{e}_3^T \end{bmatrix}^T \begin{bmatrix} \lambda_1 & 0 & 0 \\ 0 & \lambda_2 & 0 \\ 0 & 0 & \lambda_3 \end{bmatrix} \begin{bmatrix} \mathbf{e}_1^T \\ \mathbf{e}_2^T \\ \mathbf{e}_3^T \end{bmatrix} \begin{bmatrix} C_1 \\ C_2 \\ C_3 \end{bmatrix},$$

(17)

where λ_1, λ_2, and λ_3 ($\lambda_1 \geq \lambda_2 \geq \lambda_3$) are the eigenvalues for the coefficient matrix, and $\mathbf{e}_1$, $\mathbf{e}_2$, and $\mathbf{e}_3$ are unit length eigenvectors corresponding to λ_1, λ_2, and λ_3, respectively. Because R and R^2 mean robustness against noise, we propose the following parameters $\mathbf{r}_1$, $\mathbf{r}_2$, and $\mathbf{r}_3$ as reliability indices.

$$\mathbf{r}_1(r_{11}, r_{12}, r_{13}) = \sqrt{\lambda_1} \mathbf{e}_1,$$ (18)

$$\mathbf{r}_2(r_{21}, r_{22}, r_{23}) = \sqrt{\lambda_2} \mathbf{e}_2,$$ (19)

$$\mathbf{r}_3(r_{31}, r_{32}, r_{33}) = \sqrt{\lambda_3} \mathbf{e}_3,$$ (20)

where $\mathbf{r}_1$ points to the most reliable direction in the rectangular coordinate system, and $\mathbf{r}_3$ points to the most unreliable direction.

3.2 Stabilization Process

In this section, we propose a process for stabilizing the determined motion field and illumination parameter distribution using the reliability indices, $\mathbf{r}_1$, $\mathbf{r}_2$, and $\mathbf{r}_3$. Our process follows the conventional stabilization method [15]. The relaxation process described here uses the reliability indices and modifies $\mathbf{v}_{ESTO}$ estimated by ESTO. The error function E_s, which should be minimized in an image plane V, is defined as follows.

$$E_s(u, v, w) = S_r + \beta S_{s1} + \gamma S_{s2},$$ (21)

where

$$S_r = \int_V \left\{ (\mathbf{r}_1 \cdot \Delta\mathbf{v})^2 + (\mathbf{r}_2 \cdot \Delta\mathbf{v})^2 + (\mathbf{r}_3 \cdot \Delta\mathbf{v})^2 \right\} dxdy,$$ (22)

$$S_{s1} = \int_V \left\{ \left(\frac{\partial u}{\partial x}\right)^2 + \left(\frac{\partial u}{\partial y}\right)^2 + \left(\frac{\partial v}{\partial x}\right)^2 + \left(\frac{\partial v}{\partial y}\right)^2 \right\} dxdy,$$ (23)

$$S_{s2} = \int_V \left\{ \left(\frac{\partial w}{\partial x}\right)^2 + \left(\frac{\partial w}{\partial y}\right)^2 \right\} dxdy,$$ (24)

$$\Delta\mathbf{v} = (u - u', v - v', w - w').$$ (25)

S_r is a penalty function; S_{s1} and S_{s2} are stabilizing functions; β and γ are constants balancing three constraints; u', v', w' are determined in advance by ESTO using Eq. (3).

Using the calculus of variation, we can determine the unknown parameters (u, v, w). The *Euler-Lagrange* equations for the error function E_s yeild the following equations.

$$(\mathbf{r}_1 \cdot \Delta\mathbf{v}) r_{11} + (\mathbf{r}_2 \cdot \Delta\mathbf{v}) r_{21} + (\mathbf{r}_3 \cdot \Delta\mathbf{v}) r_{31}$$

$$-\beta \left(\frac{\partial^2 u}{\partial x^2} + \frac{\partial^2 u}{\partial y^2}\right) = 0,$$ (26)

$$(\mathbf{r}_1 \cdot \Delta\mathbf{v}) r_{12} + (\mathbf{r}_2 \cdot \Delta\mathbf{v}) r_{22} + (\mathbf{r}_3 \cdot \Delta\mathbf{v}) r_{32}$$

$$-\beta \left(\frac{\partial^2 v}{\partial x^2} + \frac{\partial^2 v}{\partial y^2}\right) = 0,$$ (27)

$$(\mathbf{r}_1 \cdot \Delta\mathbf{v}) r_{13} + (\mathbf{r}_2 \cdot \Delta\mathbf{v}) r_{23} + (\mathbf{r}_3 \cdot \Delta\mathbf{v}) r_{33}$$

$$-\gamma \left(\frac{\partial^2 w}{\partial x^2} + \frac{\partial^2 w}{\partial y^2}\right) = 0.$$ (28)

Using the approximation to the Laplacian [16],

$$\frac{\partial^2 u}{\partial x^2} + \frac{\partial^2 u}{\partial y^2} = \bar{u} - u,$$ (29)

$$\frac{\partial^2 v}{\partial x^2} + \frac{\partial^2 v}{\partial y^2} = \bar{v} - v,$$ (30)

$$\frac{\partial^2 w}{\partial x^2} + \frac{\partial^2 w}{\partial y^2} = \bar{w} - w,$$ (31)

Equations (26)–(28) can be written as

$$a(u' - u) + d(v' - v) + e(w' - w) + \beta(\bar{u} - u) = 0,$$ (32)

$$d(u' - u) + b(v' - v) + h(w' - w) + \beta(\bar{v} - v) = 0,$$ (33)

$$e(u' - u) + h(v' - v) + c(w' - w) + \gamma(\bar{w} - w) = 0.$$ (34)

For numerical calculation, the SOR scheme results in the following equations.

$$u^{k+1} = \xi \frac{\beta\bar{u} + au' + d\left(v' - v^k\right) + e\left(w' - w^k\right)}{a + \beta}$$
$$- (\xi - 1) u^k,$$ (35)

$$v^{k+1} = \xi \frac{\beta\bar{v} + d\left(u' - u^k\right) + bv' + h\left(w' - w^k\right)}{b + \beta}$$
$$- (\xi - 1) v^k,$$ (36)

$$w^{k+1} = \xi \frac{\gamma\bar{w} + e\left(u' - u^k\right) + h\left(v' - v^k\right) + cw'}{c + \gamma}$$
$$- (\xi - 1) w^k.$$ (37)

Superscript k represents the iteration step, and ξ represents the acceleration parameter. Practical values for ξ were 1.8 in our experiments.

This process modifies $\mathbf{v}_{ESTO}$ to directions of more reliable neighbor $\mathbf{v}_{ESTO}$s under a balance between the penalty function, S_r, and two stabilizing functions, S_{s1} and S_{s2}.

4. Experimental Results

4.1 Analysis of Synthetic Image Sequences under Non-uniform or Non-stationary Illumination

We generated two synthetic image sequences by simulating non-uniform and non-stationary illuminations with a translation of a static scene (Figs. 2, 3). The generated image sequences consisted of 128 × 128 (pixels) and 10 (frames).
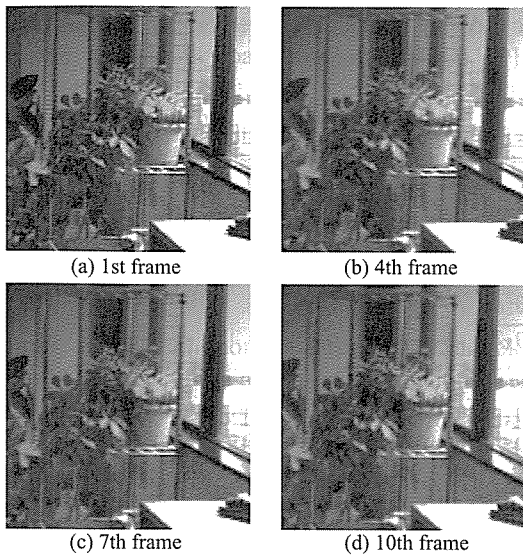
Fig. 2   A synthetic image sequence, f_1, under non-uniform illumination, p_1.
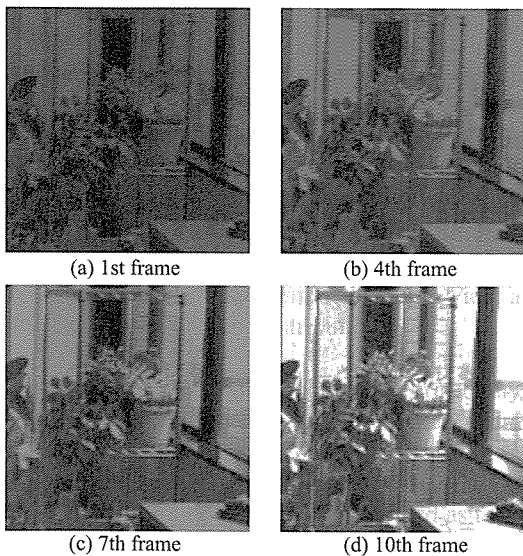
Fig. 3   A synthetic image sequence, f_2, under non-stationary illumination, p_2.

The brightness was quantified into 256 (levels). The image sequences had a uniform motion vector $\mathbf{v} = (-0.8, 0.3)$ (pixels/frame). An image function $f_0(x, y, t)$ of the original translation image sequence was modified by non-uniform illumination $p_1(x, y)$ and non-stationary illumination $p_2(t)$.

$$p_1(x, y) = \frac{x + y}{127 + 127}, \tag{38}$$

$$p_2(t) = 0.1 \exp(0.2t). \tag{39}$$

The image sequence under non-uniform illumination $f_1(x, y, t)$ and the image sequence under non-stationary illumination $f_2(x, y, t)$ were represented by the following equations.

$$f_1(x, y, t) = f_0(x, y, t) p_1(x, y), \tag{40}$$

$$f_2(x, y, t) = f_0(x, y, t) p_2(t). \tag{41}$$

Since the theoretical illumination parameter distribution w is expressed as

$$w = \mathbf{v} \cdot \frac{\nabla p_1}{p_1} + \frac{\partial p_2 / \partial t}{p_2}, \tag{42}$$

the correct illumination parameter distributions of f_1 and f_2 are described as $w = (-0.8 + 0.3)/(x + y)$ and $w = 0.2$, respectively [5].

We applied three methods to the synthetic image sequences: ESTO, ESTO with the Ohta's stabilization method, and ESTO with the proposed method. The Ohta's stabilization method wasn't designed for ESTO. However, if we assume that the illumination parameter distribution determined by ESTO is correct, we can use the following equation instead of Eq. (8),

$$R = \frac{\| F_t + \sum_{l=0}^{L-1} \sum_{m=0}^{M-1} (fw) \|}{A}. \tag{43}$$

The Ohta's stabilization method can be applied to any result of ESTO using the Eq. (43). Of course, the Ohta's stabilization method cannot stabilize the illumination parameter distribution determined by ESTO.

We used spatial and temporal domains of $L \times M = 3 \times 3$ (pixels) and $N = 8$ (frames) for each method. In the Ohta's stabilization method, we used $\alpha = 1000$, and 50 iterations. In the proposed stabilization method, we used $\beta = 1000$, $\gamma = 50000$, and 50 iterations.

The determined motion fields and illumination parameter distributions of image sequences f_1 (non-uniform illumination), and f_2 (non-stationary illumination) are shown in Figs. 4, 5, 6, 7. The results of original ESTO showed miss-detections of the motion fields at poorly textured areas, and at the edges of some objects (see Figs. 4 (a), 6 (a)). These also showed large errors of the illumination parameter distribution at almost dark objects, and at edges of some objects (see Figs. 5 (a), 7 (a)). These errors of the motion fields and the illumination parameter distributions were observed at similar areas in two image sequences, f_1 and f_2, regardless of difference of the illumination conditions. The results indicated that the image pattern and brightness of these image sequences were the cause of these errors. The results of the Ohta's stabilization method showed better motion fields (see Figs. 4 (b), 6 (b)). However, the determined illumination parameter distributions were the same as the results of ESTO (see Figs. 5 (a) (b), 7 (a) (b)). On the other hand, the proposed method led to better motion fields and illumination parameter distributions (see Figs. 4 (c), 5 (c), 6 (c), 7 (c)). Since we used the reliability indices estimated from the image pattern and brightness of these image sequences, the miss-detections at non-reliable areas were easier modified than motion fields at reliable areas.

Now we try to verify the accuracy of these methods quantitatively. For an index of error measurement, we used angular measure of error proposed by Barron et al. [1]. They evaluated the error between the correct velocity $\mathbf{v}_c = (u_c, v_c)$
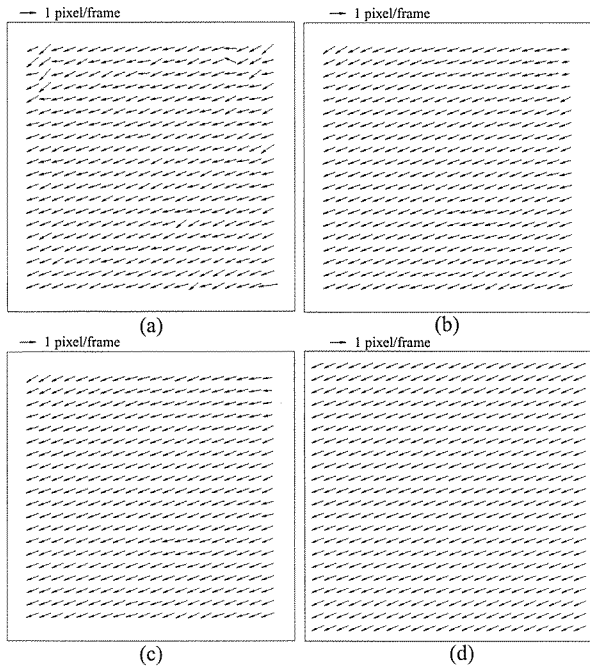
Fig. 4 Motion fields determined by: (a) ESTO, (b) ESTO with the Ohta's stabilization method, and (c) ESTO with the proposed stabilization method from the image sequence under non-uniform illumination (Fig. 2). (d) Theoretical motion field.

Fig. 6 Motion fields determined by: (a) ESTO, (b) ESTO with the Ohta's stabilization method, (c) ESTO with the proposed stabilization method from the image sequence under non-stationary illumination (Fig. 3). (d) Theoretical motion field.

-0.1   0   0.1
w
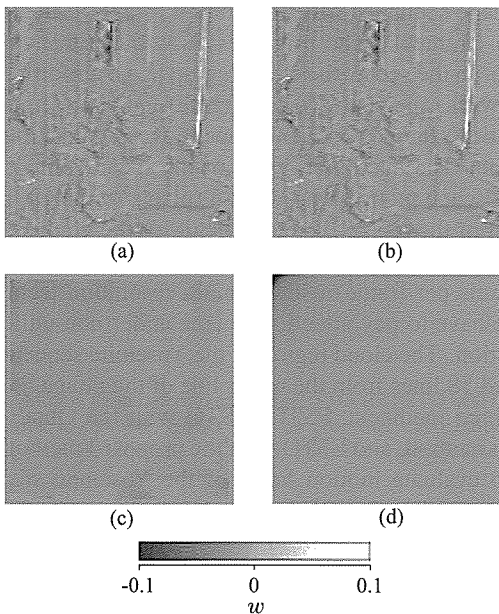
Fig. 5 Illumination parameter distributions determined by: (a) ESTO, (b) ESTO with the Ohta's stabilization method, and (c) ESTO with the proposed stabilization method from the image sequence under non-uniform illumination (Fig. 2). (d) Theoretical illumination parameter distribution, $w = (-0.8 + 0.3)/(x + y)$.

0   0.2   0.4
w
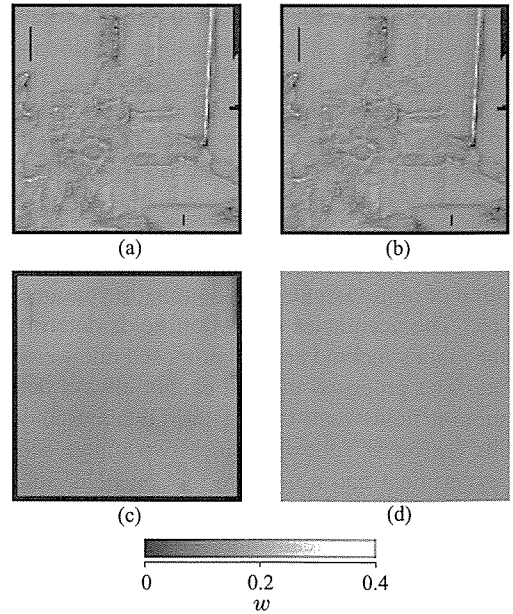
Fig. 7 Illumination parameter distributions determined by: (a) ESTO, (b) ESTO with the Ohta's stabilization method, (c) ESTO with the proposed stabilization method from the image sequence under non-stationary illumination (Fig. 3). (d) Theoretical illumination parameter distribution, $w = 0.200$.

and the determined $\mathbf{v}_e = (u, v)$ as the angle between the unit vectors ($\mathbf{v}_{3c}$ and $\mathbf{v}_{3e}$) in 3-dimensional space. The definitions of the vectors are as follows.

$$\mathbf{v}_{3c} \equiv \frac{1}{\sqrt{u_c^2 + v_c^2 + 1}} (u_c, v_c, 1), \tag{44}$$

$$\mathbf{v}_{3e} \equiv \frac{1}{\sqrt{u^2 + v^2 + 1}} (u, v, 1). \tag{45}$$

Table 1 Comparison of angular errors E_p and illumination parameter distribution errors E_w determined from two image sequences under non-uniform illumination, f_1 (Fig. 2), and non-stationary illumination, f_2 (Fig. 3).

Image sequence	Method	Error E_p	Error E_w
f_1	ESTO	3.06	1.56
	ESTO + Ohta's stabilization	1.70	1.56
	ESTO + proposed stabilization	1.88	0.66
f_2	ESTO	6.24	0.106
	ESTO + Ohta's stabilization	2.28	0.106
	ESTO + proposed stabilization	2.48	0.077

They defined the angular error E_p between the correct vector $\mathbf{v}_{3c}$ and the determined $\mathbf{v}_{3e}$ by

$$E_p = \frac{1}{N_x N_y} \sum_{x=0}^{N_x-1} \sum_{y=0}^{N_y-1} \arccos\{\mathbf{v}_{3c}(x,y) \cdot \mathbf{v}_{3e}(x,y)\}, \quad (46)$$

where N_x and N_y (pixels) were the sizes of the image sequence, but all points that cannot be evaluated were removed from this calculation.

The error of the determined illumination parameter distribution $w_e(x, y)$ was evaluated by the following equation:

$$E_w = \frac{1}{N_x N_y} \sum_{x=0}^{N_x-1} \sum_{y=0}^{N_y-1} \frac{|w_c(x, y) - w_e(x, y)|}{|w_c(x, y)|}, \quad (47)$$

where $w_c(x, y)$ was a correct illumination parameter distribution.

These errors are summarized in Table 1, which shows the quantitative superiority of the proposed method for determination of motion fields and illumination parameter distributions. The accuracies of motion fields determined by use of the Ohta's method and the proposed one were almost the same. The proposed method cannot always determine better motion fields than that of the Ohta's method. We think this reason as follows. Since two image sequences in this experiment had a uniform motion field, stabilizing methods have to modify the motion field more smoothly to get better results. Meanwhile, there were many errors in these illumination parameter distributions determined by ESTO. Modification of these distribtuions with the proposed method increased the value of the penalty function S_r (see Eq. (22)). In the Ohta's method, there is not the function for modification of the distributions. Therefore, the proposed method could not modify the motion fields smoother than the Ohta's method, because the constants, α and β, balancing the penalty functions and the stabilizing functions were used the same value in these methods.

4.2 Analysis of a Standard Image Sequence

In this section, we consider a famous Yosemite sequence

(a) 1st frame   (b) 5th frame

(c) 9th frame   (d) 13th frame
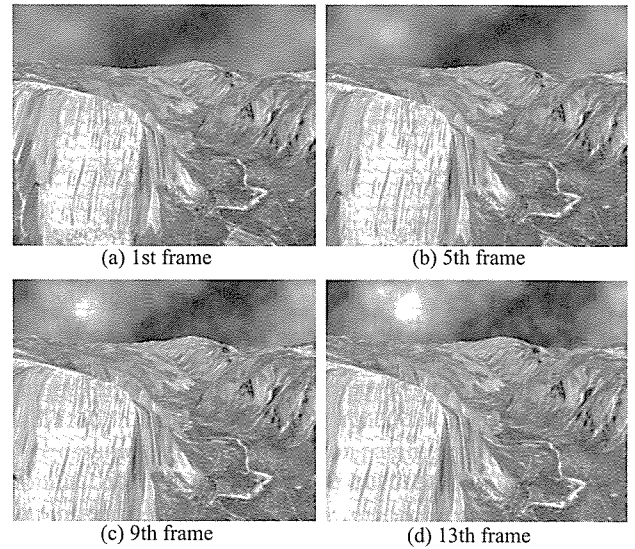
Fig. 8 The Yosemite sequence.

obtained from the ftp server, *ftp.csd.uwo.ca*, because the Yosemite sequence is commonly used for testing the performance of many methods [1], [5], [9]. We focus our attention only on accuracies of determined motion fields.

Figure 8 shows snapshots of the Yosemite sequence. The image sequence had a resolution of 316×252 (pixels) and 15 (frames). The brightness was quantified into 256 (levels). In the scene, the cloud region had a uniform motion vector with a speed of 2 (pixels/frame) and had a temporal illumination change. The landscape moved against the depth direction. The maximum value of the speed component of the landscape motion was about 5 (pixels/frame) at the bottom left of the image. It was difficult for the gradient-based approach to determine a large motion vector (more than several pixels per frame) without multi-resolution techniques, and we have to pay attention to area under non-uniform illumination. The cloud region of the Yosemite sequence was trimmed 58 lines from the upper line of the image.

Three methods: ESTO, ESTO with the Ohta's stabilization method, and ESTO with the proposed method, were used to evaluate motion fields of the Yosemite sequence, and the cloud region of the Yosemite sequence. The size of the spatial domain $L \times M$ was 7×7 (pixels) and that of the temporal domain N was 13 (frames) in the local optimization of ESTO. In the Ohta's stabilization method, we used $\alpha = 1000$, and 50 iterations. In the proposed stabilization method, we used $\beta = 1000$, $\gamma = 50000$, and 50 iterations. The determined motion fields and illumination parameter distributions of the Yosemite sequence are shown in Figs. 9, 10.

The error comparisons are summarized in Table 2, and Table 3. Table 3 picked up an error comparison of motion field determined only from the cloud region of the Yosemite sequence. The proposed method and the Ohta's stabilization method were effective in decreasing errors of the determined motion fields. The accuracies of the both methods were

– 2 pixels/frame

(a)

– 2 pixels/frame

(b)

– 2 pixels/frame

(c)

– 2 pixels/frame

(d)
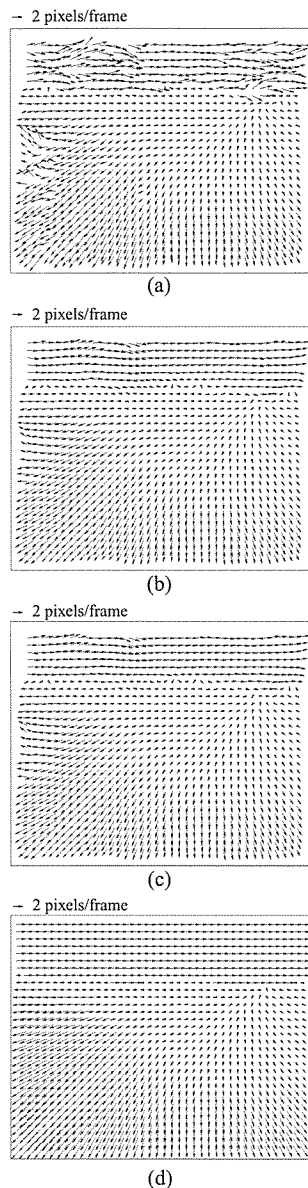
Fig. 9　Motion fields determined by: (a) ESTO, (b) ESTO with the Ohta's stabilization method, (c) ESTO with the proposed stabilization method from the Yosemite sequence (Fig. 8). (d) Theoretical motion field.

(a)　　　　　　　　　　(b)

-0.1　　　0　　　0.1
w
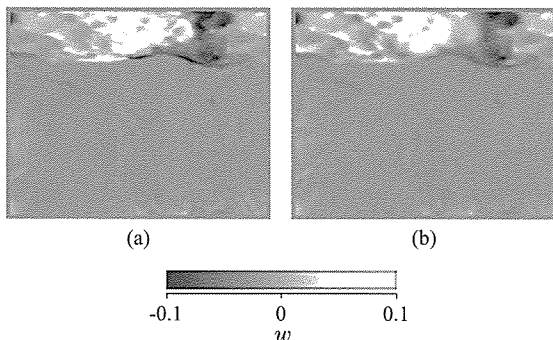
Fig. 10　Illumination parameter distributions determined by: (a) ESTO with the Ohta's stabilization method, (b) ESTO with the proposed stabilization method from the the Yosemite sequence (Fig. 8).

Table 2　Comparison of angular errors E_p determined from the Yosemite sequence (Fig. 8).

Method	Error E_p
ESTO	8.15
ESTO + Ohta's stabilization	6.90
ESTO + proposed stabilization	6.90

Table 3　Comparison of angular errors E_p determined from a cloud region of the Yosemite sequence.

Method	Error E_p
ESTO	11.8
ESTO + Ohta's stabilization	7.38
ESTO + proposed stabilization	7.09

almost the same for the Yosemite sequence and the cloud region of the Yosemite sequence. The proposed method showed the best accuracy for the Yosemite sequence [1], [5]. The proposed method stabilizes not only motion fields but also illumination parameter distributions.

5. Conclusion

We proposed a post-processing method that can simultaneously stabilize a motion field and an illumination parameter distribution. The first candidates of the motion field and the distribution are ditermined by ESTO. The distribution indicates illumination conditions in image sequences, e.g. non-uniform illumination and non-stationary illumination. The proposed method succeeded in simultaneous evaluation of accurate motion fields and illumination parameter distributions, especially at poorly textured areas, at edges of objects, and at almost black objects in images.

References

[1] J.L. Barron, D.J. Fleet, and S.S. Beauchemin, "Systems and experiment — Performance of optical flow techniques," Int. J. Comput. Vis., vol.12, no.1, pp.43–77, 1994.

[2] J.W. Brandt, "Improved accuracy in gradient-based optical flow estimation," Int. J. Comput. Vis., vol.25, no.1, pp.5–22, 1997.

[3] S. Lai and B.C. Vemuri, "Reliable and efficient computation of optical flow," Int. J. Comput. Vis., vol.29, no.2, pp.87–105, 1998.

[4] A. Bab-Hadiashar and D. Suter, "Robust optic flow computation," Int. J. Comput. Vis., vol.29, no.1, pp.59–77, 1997.

[5] L. Zhang, T. Sakurai, and H. Miike, "Detection of motion fields under spatio-temporal non-uniform illumination," Image Vis. Comput., vol.17, pp.307–318, 1999.

[6] M. Ye and R.M. Haralick, "Local gradient, global matching, piecewise-smooth optical flow," Proc. 2001 IEEE Conf. on Computer Vision and Pattern Recognition, pp.II712–II717, 2001.

[7] A. Nomura, H. Miike, and K. Koga, "Determining motion fields under non-uniform illumination," Pattern Recognit. Lett., vol.16, pp.285–296, 1995.

[8] N. Mukawa, "Optical model-based analysis of consecutive images," Comput. Vis. Image Underst., vol.66, pp.25–32 1997.

[9] A. Nomura, "Spatio-temporal optimization method for determining

motion vector fields under non-stationary illumination," Image Vis. Comput., vol.18, pp.939–950, 2000.

[10] H.W. Haussecker and J. Fleet, "Computing optical flow with physical models of brightness variation," IEEE Trans. Pattern Anal. Mach. Intell., vol.23, no.6, pp.661–673, 2001.

[11] E. Dubois and J. Konrad, "Estimation of 2D motion fields from images sequences with application to motion compensated processing," in Motion analysis and image sequence processing, pp.53–87, Kluwer Academy Publishers, Dordrecht, 1993.

[12] M. Shizawa and K. Mase, "Multiple optical flow — Fundamental constraint equations and unified computational theory for detecting motion transparency and motion boundaries," IEICE Trans. Inf. & Syst. (Japanese Edition), vol.J76-D-II, no.5, pp.987–1005, May 1993.

[13] A. Verri, F. Girosi, and V. Tore, "Differential techniques for optical flow," J. Opt. Soc. Am., vol.A7, pp.912–922, 1990.

[14] A. Nomura, H. Miike, and E. Yokoyama, "Detecting motion and diffusion from a dynamic image sequence," IEEJ Trans. EIS, vol.115-C, pp.403–409, 1995.

[15] N. Ohta, "Image movement detection with reliability indices," IEICE Trans., vol.E74, no.10, pp.3379–3388, Oct. 1991.

[16] B.K.P. Horn and B.G. Schunck, "Determining optical flow," Artif. Intell., vol.17, pp.185–203, 1981.

[17] J.K. Kearney, W.B. Thompson, and D.L. Boley, "Optical flow estimation: An error analysis of gradient-based methods with local optimization," IEEE Trans. Pattern Anal. Mach. Intell., vol.9, pp.229–244, 1987.

[18] A. Nomura, H. Miike, and K. Koga, "Field theory approach for determining optical flow," Pattern Recognit. Lett., vol.12, pp.183–190, 1991.

[19] T. Hara, T. Kudou, H. Miike, E. Yokoyama, and A. Nomura, "Recovering 3D-shape from motion stereo under non-uniform illumination," Proc. IARP MVA'96, pp.241–244, 1996.

[20] K. Nakajima, A. Osa, T. Maekawa, and H. Miike, "Evaluation of body motion by optical flow analysis," Jpn. J. Appl. Phys., vol.36, pp.2929–2937, 1997.
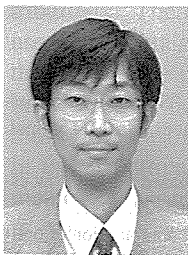
Atsushi Osa received the B.E. and M.E. degrees in electrical and electric engineering from Yamaguchi University, Japan in 1995 and 1997. He is currently a research associate at Yamaguchi University. His research interests include computer vision, computer graphics, nonlinear sciences, and design engineering. He is a member of the Information Processing Society of Japan, Japan Society of Image Arts and Sciences, and the Society for Art and Science.

Hidetoshi Miike received the B.E. degree in 1971, the M.E. degree in 1973, and the Dr. Eng. degree in electronics in 1976, all from Kyushu University, Japan. In 1976, he joined Faculty of Engineering, Yamaguchi University. Since 1991, he has been a professor of the university. His research interests include nonlinear sciences and fluid dynamics. He is a member of the Information Processing Society of Japan, the Physical Society of Japan, IEEE computer society, and the American Association for the Advancement of Science.